Trends in Biotechnology

CellPress REVIEWS

Review

3D Quantitative Chemical Imaging of Tissues by Spectromics

Cyril Petibois[1,2,*]

Mid-infrared (IR), Raman, and X-ray fluorescence (XRF) spectroscopy methods, as well as mass spectrometry (MS), can be used for 3D chemical imaging. These techniques offer an invaluable opportunity to access chemical features of biological samples in a nonsupervised way. The global chemical information they provide enables the exploitation of a large array of chemical species or parameters, so-called 'spectromics'. Extracting chemical data from spectra is critical for the high-quality chemical analysis of biosamples. Furthermore, these are the only currently available techniques that can quantitatively analyze tissue content (e.g., molecular concentrations) and substructures (e.g., cells or blood vessels). The development of chemical-derived biological metadata appears to be a new way to exploit spectral information with machine learning algorithms.

Spectromicroscopy of Biological Samples

Tomography (see Glossary) was a technological breakthrough first reported in 1979, and tomography image reconstruction methods have been extensively developed since this initial report. Magnetic resonance imaging (MRI) and X-ray computed tomography (CT) are well-known examples of such methods. They provide a 3D visualization of organs, which can depict anatomical features that are of diagnostic value. However, in smaller biosystems, such as cells, tissues, or small-animal organs, these techniques are limited by their resolution and sensitivity. Thus, there is a lack of reliable 3D imaging solutions at the microscopic scale for use in biological analysis [1]. Fluorescence-based imaging techniques can perform 3D analyses on small biosamples, mostly cells and small tissue blocks, but their penetration depth is limited (Table 1) and the use of labels restricts the analytical value of the 3D images [2]. This is a major frontier in biological research, where supervised techniques depending on labels or contrast agents can no longer satisfy the discovery appetite for biospecimens. Better-quality images of biosamples, at higher resolution, with higher contrast, and providing larger quantities of information, makes the addition of global chemical information more important. This is particularly true when several (or a multitude of) chemical compounds of tissues need to be revealed by histology (Box 1).

The first issue with spectromicroscopies is that there is a mismatch between their intrinsic analytical capabilities and the requirements of histological analyses, which require sample information at the 5–10-μm spatial resolution for a 1 mm^3–1 cm^3 tissue volume. They can achieve better lateral resolution, but their penetration depth is much less than 1 mm. Additionally, analytical performances must be balanced over the limits of scanning duration to obtain a signal:noise ratio (S/N) allowing high-quality spectral data treatments. These requirements define the practical performances of these analytical methods, which have been reviewed for different 2D application cases [3–6], but never for 3D histological analyses. Four

Trends

3D chemical imaging is achieved by several spectromicroscopic methods. These provide a quantitative analysis of tissue content and substructures with a depth of information that no other histological technique can determine from the same sample. However, they are currently underexploited despite their potential.

Standardization of spectral data acquisition and treatments is the next frontier in the development of 3D chemical imaging routines. This methodological effort is required to advance the development of reliable analytical tools for the biosciences and industry.

Spectromics is emerging as a new trend for nonsupervised and automated data treatment from 3D spectrum matrices. It has the advantages of being able to use all the chemical information available from spectra and of interpretability, since spectral data can be converted into biological metadata.

[1]University of Bordeaux, Inserm U1029 LAMC, Allée Geoffroy Saint-Hilaire Bat. B2, F33600 Pessac, France
[2]Academia Sinica, Institute of Physics, 128 Sec. 2, Academia Road, Nankang, Taipei 11529, Taiwan, Republic of China

*Correspondence: cyril.petibois@u-bordeaux.fr, petibois@gate.sinica.edu.tw (C. Petibois).

spectromicroscopy techniques have been shown to achieve 3D **chemical imaging** of tissues: IR spectroscopy [7–10], Raman spectroscopy [11–13], MS [11,14–16], and XRF [17–19].

These spectromicroscopies cannot rival fluorescence-based imaging techniques in terms of resolution and penetration depth. However, in terms of sample area scanned per unit of time (in minutes), IR and MS match the performance of multiphoton microscopy. Thus, with appropriate 3D reconstruction methods, a 3D view can be achieved; the advantage of spectromicroscopies stems from their ability to provide many different chemical data compared with the two or three labels possible with multiphoton microscopy. Finally, the main advantages of spectromicroscopies are that they can provide extensive, if not global, quantitative chemical information about the sample without *a priori* supervision (compared with label-related histology).

Which Method to Choose for the 3D Chemical Imaging of Tissues?

The choice of a spectromicroscopy method for chemical imaging of a tissue block will depend on a compromise between three resolutions (spectral, lateral for 2D, and spatial for 3D), the kind of chemical species to investigate, and the targeted sensitivity. In terms of 3D analyses by spectromicroscopies, a few studies have shown that tomographic analysis can be directly performed on small biosamples, such as intact hair with synchrotron radiation for IR microscopy [8], confocal Raman microscopy for living cells [13], or XRF microscopy of zebrafish embryo [17], also using a synchrotron radiation source. These tomographic imaging methods have been made possible within the limits of the penetration depth for each technique (i.e., before total photon absorption is reached). The ability to analyze larger objects in the future could come from the use of more-intense light sources, but this is largely compromised by the ionizing radiation induced by X-rays for 3D-XRF imaging or sample heating induced by more-intense lasers used in 3D-Raman imaging [20]. High radiation doses or laser heating will deeply modify the chemical content of tissues, such as the loss of protein native conformations, nucleic acid fragmentation, lipid transesterification, and so on, which will also strongly modify the chemical information contained in the spectra. The development of more-sensitive or 'zero-noise' detectors [21] is also expected to extend the application field of tomographic imaging by spectromicroscopies, but it will not allow the analysis of bigger samples. In general, the volumetric limit of these tomographic methods is less than 1 mm^3 and, thus, insufficient for 3D histology.

Therefore, for 3D chemical analysis of large tissue samples with spectromicroscopies, it is necessary to split the sample into fractions that can be further reconstructed as a 3D volume. For soft tissues, this is mainly performed by continuous sectioning, although MS imaging (MSI) uses laser ablation for time-of-flight scanning ion-MS (ToF-SIMS). Then, a transmission measurement combined with laterally resolved scanning can quantitatively analyze the chemical content. Computing techniques can produce 3D stacks of successive 2D images of a tissue block or an organ that have been continuously sectioned, dyed, or stained, imaged, and segmented for 3D visualization [22]. However, for spectromicroscopies, it is preferable to use fresh tissue sections, unmodified by staining or embedding methods, to ensure that the native chemical composition of the sample is maintained before analysis [23].

Once organized as a **3D spectrum matrix** representing the 'spectral image' of the sample, spectra can be processed to extract chemical information. The methods for data extraction vary between spectroscopy techniques (Figure 1). However, before the chemical data are extracted from the spectra, it is also important to take into account the nature of the spectral data, revealed as peaks or bands, which have shapes that can be described mathematically. Raman and IR spectroscopies provide sharp and large bands, respectively, while XRF spectroscopy and MS provide sharp peaks. Therefore, mass and XRF spectroscopies provide

Glossary

3D spectrum matrix: a set of spatially organized spectra that represents the raw chemical information about a sample volume.
Biological metadata: biological content that is reconstructed from another source of sample information (chemical, anatomical, etc.).
Chemical imaging: imaging a sample from a light-matter interaction (typically absorption, reflection, and transmission; but also exploiting the size or mass of molecules or their fragments) that reveals its chemical composition.
Nonsupervised analysis: use of statistical methods that perform the comparison between samples based on all the sample information available. The more information available, the better the ability of multivariate statistics will be to discriminate between samples.
Spectromics: the use of all the available information in spectra for characterizing a sample. Similar to any other 'omic', its aim is the collective characterization and quantification of pools of chemical data that translate into the sample contents (substructures, cells, molecules, etc.).
Tomography: imaging a sample by sections or sectioning through the use of any kind of penetrating wave. It requires co-adding projections from several visualization angles to reconstruct the internal structure of the sample in 3D. However, this does not require the physical sectioning of the sample.

Table 1. Typical Analytical Performances of Spectromicroscopies for Chemical Imaging of Soft Tissues[a]

Technique	Penetration depth (μm)	Lateral resolution (μm)	Z-axis resolution (μm)	Spectral interval, (resolution)	Field of view (μm × μm)	Tissue area covered/min (μm^2)	Accessible chemical data (*n*)	Refs
Confocal imaging	500	0.2	1	None	200 × 200	160 000 000 000	Individual	[2]
Multiphoton microscopy	1000	0.3	0.5	None	200 × 200	1 000 000	Up to 3	[2]
Multiphoton with clearing	5000	0.3	0.3	None	200 × 200	1 000 000	Up to 3	[2]
IR	30	5–10	None	500–4000 cm^{-1} (2–8 cm^{-1})	2000 × 2000	800 000	100–200	[10,25]
Raman confocal	50	4–32	0.08–0.50	100–4000 cm^{-1} (0.5–4 cm^{-1})	Single point volume	70 000	50–100	[2,13]
MS	0.01	10–100	None	500–10 000 m/z, (1–10 m/z)	Single point volume	1 500 000	100–1000	[45,48]
XRF	20	5–20	None	1–60 keV (0.1–0.5 keV)	10 000 × 10 000	100 000	5–20	[17,55]

[a]These values take into account the expectation of histological analyses, which require usually a microscopic resolution of 1–10 μm from tissue sections of 4–20 μm thickness. Fluorescence imaging techniques are included to compare the analytical performances of 3D chemical imaging techniques with the current gold standards of 3D histological analyses.

chemical data with more accurate identification. XRF spectroscopy is favorable because elements can be easily identified, although the number of peaks is limited. Given the high sensitivity of MS, m/z spectra can reveal hundreds of peaks. Raman spectroscopy is the least-sensitive vibrational spectroscopy technique discussed here, but identifying chemical contents is easier than for IR because of sharper bands. In turn, IR spectroscopy is more sensitive and provides more chemical data, but the overlap between bands is more pronounced.

3D-IR Spectromicroscopy

IR microscopy has long been powered by IR interferometers, thus requiring a Fourier transform of the interferogram to obtain IR spectra. Since 1986, this technique has been known as 'FTIR spectrometry' or 'FTIR spectromicroscopy' when associated to a microscope. Two major technological developments have paved the way towards its better analytical

Box 1. Analytical Supervision, Chemical Imaging, and Spectromics

A supervised technique uses labels or contrast agents to highlight chosen sample contents. By contrast, nonsupervised techniques do not use labels or contrast agents but instead use the natural contrast of the sample. For example, chemical imaging is the analytical ability to create a visual image of the distribution of components based on simultaneous measurements of spectral and spatial information (to which can be added temporal information). This analytical domain might be extended to chemical information from contrast agents, such as radionuclides for positron-emission tomography (PET). However, in this instance, one piece of information is collected, the contrast agent, while spectroscopies offer an array of chemical data from collected spectra. For the chemical imaging of biosamples, spectroscopies produce spectral data from the interaction of light (mainly IR, ultraviolet, or X-rays) or ions (ion-MS) with matter, and the results depend on the composition of the biosample. With spectroscopies, chemical imaging covers two major fields: hyperspectral imaging, which measures contiguous spectral bands (IR spectroscopy, for example), and multispectral imaging, which measures spaced spectral bands from different regions of the electromagnetic spectrum. With contiguous spectral bands, deconvolution techniques must be applied to separate chemical data. The spectroscopies currently used for the chemical analysis of biosamples are known as hyperspectral techniques. When they are coupled to a microscope or when they can laterally scan a sample, they are called 'spectromicroscopies' and provide a laterally resolved chemical analysis of the biosample. When used to extract all the chemical data provided in spectra, spectroscopies open the way to nonsupervised analyses of biosamples, so-called 'spectromics': this is the nonsupervised exploitation of chemical data without *a priori* understanding to compare samples or conditions.

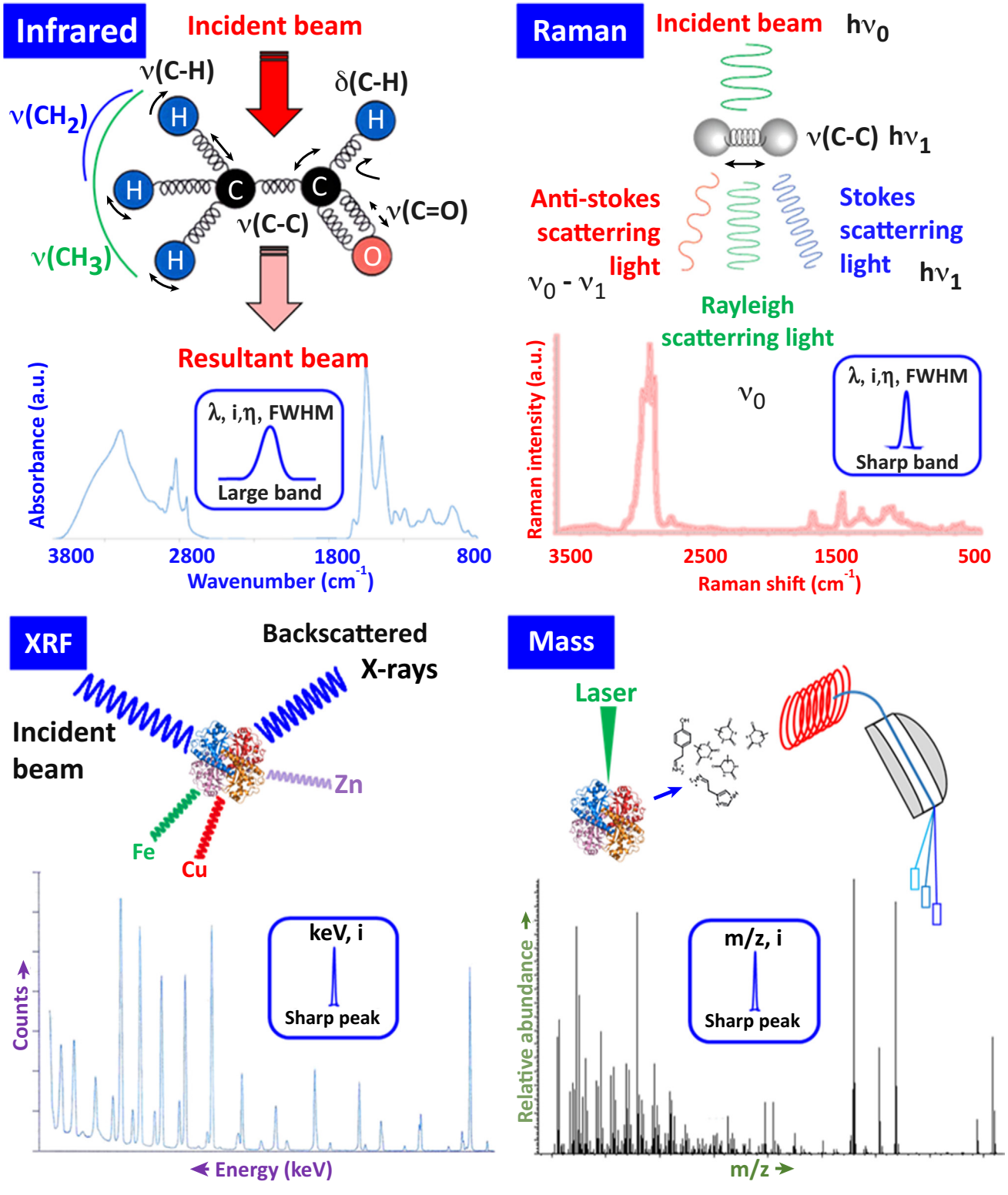

Figure 1. Physical Principles of Spectromicroscopy Methods Providing Global Chemical Information from Tissues. The infrared (IR) and Raman bands can be described by their position (λ), intensity (i), full width at half height (FWHH), and Gaussian/Lorentzian fraction (η). The mass and XRF peaks are described by their

(Figure legend continued on the bottom of the next page.)

performance: first, the use of focal plane array (FPA) detectors, introduced in 1995, and second, the advent of powerful IR sources with quantum-cascade lasers (QCLs) in 2014. Now, IR spectromicroscopy can produce millions of IR spectra per hour with high S/N. This innovation has led to new developments in IR image analyses for biosamples, such as high-speed discrete frequency infrared (DFIR) imaging to obtain stain-free biochemical images of tissue sections in minutes [24], or even 3D-IR image reconstructions for the quantitative analysis of metabolic or biochemical parameters [25].

The 3D-IR image reconstruction from a stack of consecutive 2D-IR images faces several technical issues. The complete sectioning of a mouse brain at a thickness of 20 μm generates approximately 350–400 sections and, thus, the same number of 2D-IR images. As recently described [25], it is impossible to reliably analyze so many tissue sections with FTIR instruments, which were found to be too slow for the acquisition of 2D-IR images at a resolution close to the diffraction limit. For example, a mouse brain section approximately 8 mm in diameter, with 100 scans at 4 cm^{-1} and a desired S/N of approximately 100–150, would require 80–100 h of acquisition time. It is not possible to maintain the S/N stably over these long acquisition periods. Comparatively, QCL-IR microscopes speed up the acquisition process by a factor of 50. It is obvious that the background conditions and S/N level can be more easily maintained for 2 h compared with 100 h. As a consequence, while FTIR imaging can be used to analyze small tissue blocks (<1 mm^3) to resolve tissue substructures [26], QCL-IR imaging enables the analysis of larger tissue volumes, up to a whole mouse brain [25] (Figure 2).

These first 3D-IR image reconstructions of tissue substructures were possible as a result of recent developments [27,28] in baseline corrections for normalizing IR spectral absorptions before performing reliable curve-fitting procedures. There is no universal tool for curve-fitting a spectrum comprising widely overlapping bands [29]; thus, the number of bands that can be extracted from it is indefinable in the absence of a robust mathematical model [30]. However, several studies have shown that spectral intervals can be exploited to extract IR bands that have been clearly identified for fatty acyl chains in the 3050–2800 cm^{-1} spectral interval [31,32], and for the secondary structure of proteins containing amide 1 (1720–1600 cm^{-1} spectral interval [33–35]), among others.

In the future, and for all the spectromicroscopies, the complete curve-fitting of spectra might represent a major advance in the extraction of chemical data for the analysis of tissue sample content. Interestingly, all of the peaks identified at the surface of a second derivative IR spectrum can be also revealed by automatic curve-fitting [27], but this strategy provides four times more chemical data (Figure 2). This observation justifies pursuing the standardization of this spectral data treatment to extract the largest series of chemical data from spectra. As shown by a few recent studies, blood vessels [26], cell phenotypes [36], fibrotic tissue [23], and extracellular matrix [37], to name a few, can be recognized in tissues with appropriate spectral data treatments.

intensity (i) at given mass:charge ratio (m/z) or energy (keV) levels, respectively. Therefore, X-ray fluorescence (XRF) and mass spectra (MS) only require the identification or localization of the peaks and calibration of their intensity scale to extract quantitative information. Due to the nature of the spectral data (i.e., bands, of IR and Raman spectroscopies), the spectral data treatments will be more sophisticated. This is due to the large overlap between adjacent bands for complex biological sample spectra, meaning that using the intensity at a given λ is rarely characteristic of a single band. This phenomenon is even more pronounced for IR spectroscopy, which provides large absorption bands. Thus, depending on the bands expected from spectra, Raman and IR spectroscopies will need to use second-derivative or curve-fitting methods [29]. While analyzing frozen tissues, the main analytical performances vary by technique: IR (section thickness: 5–25 μm; best 3D resolution: 10 μm; sensitivity: +++); Raman (section thickness: 5–40 μm; best 3D resolution: 5 μm; sensitivity: ++); MS (section thickness: 5–50 μm; best 3D resolution: 10 μm; sensitivity: ++++); and XRF (section thickness: 5–25 μm; Best 3D resolution: 10 μm; sensitivity: +).

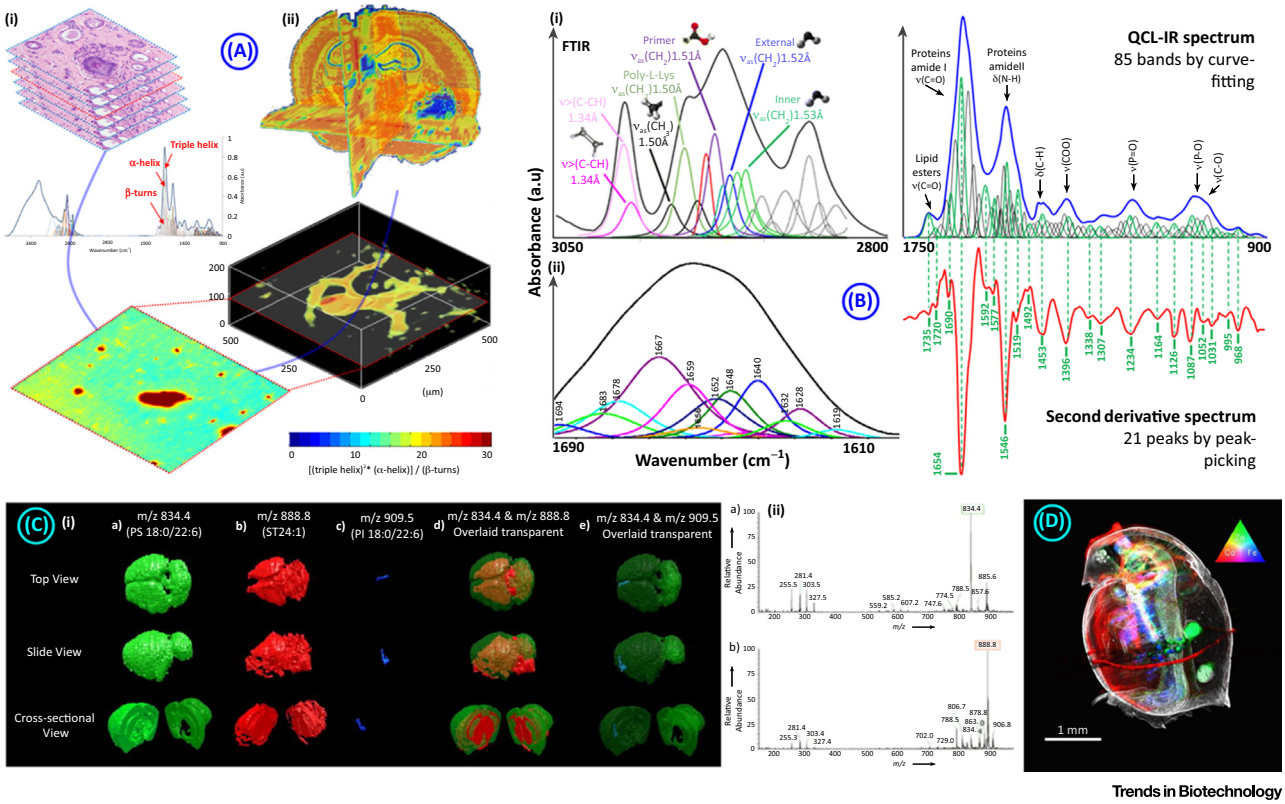

Trends in Biotechnology

Figure 2. Examples of 3D Tissue Spectromicroscopy Techniques. (A) 3D-infrared (IR) imaging of small tissue substructures and a whole mouse brain. (i) Biological metadata (here blood capillaries) can be reconstructed based on extracted spectral data (here using major absorptions from the collagen-rich basal membrane of blood vessels, triple helix absorption at 1637 cm^{-1} and α-helix absorption at 1656 cm^{-1}). This analytical concept can be systematized to the whole brain to reconstruct the microvascular network. (ii) 3D visualization of mouse brain anatomy based on the lipid:protein absorption ratio [∫(3020–2800 cm^{-1})/∫(1705–1480 cm^{-1})] for 370 consecutive tissue sections. (B) IR spectra curve-fitting for extracting individual IR absorption bands. (i) Curve-fitting of the 3050–2800 cm^{-1} spectral interval for a typical membrane phospholipid [31]. (ii) Classical curve-fitting result obtained for the amide I spectra interval, revealing the secondary structure parameters of proteins, among others. Complete curve-fitting of the IR spectrum fingerprint region (1800–900 cm^{-1}) can produce 80–100 individual bands depending on the precision of the mathematical model used. Thus, it can provide more chemical parameters than peak-picking on a second derivative spectrum (85 versus 21 chemical structures in this example of IR spectrum of a brain tissue). (C) Mouse brain 3D image by desorption electrospray ionization (DESI)-MS imaging. (i) top, side, and cross-sectional views are shown for the 3D construction of the distribution of (a) PS 18:0/22:6 in green, (b) ST 24:1 in red, and (c) PI 18:0/22:6 in blue. The same views are shown for the transparent overlaid distributions of the lipids (d) PS 18:0/22:6 and ST 24:1 and (e) PS 18:0/22:6 and PI 18:0/22:6. (ii) DESI mass spectrum obtained from a 20-mm-thick mouse brain coronal section at Bregma: −1.060 mm in the (a) gray matter and (b) white matter region. The most intense ion present in the gray matter at m/z 834.4 was identified as PS 18:0/22:6. In the white matter, the most intense ion at m/z 888.8 was identified as ST 24:1. (D) Volume rendering of a *Daphnia magna* sample. The full 3D absorption reconstruction of the daphnid (3-μm resolution) was obtained by a micro-computed tomography (CT) system. Two RGB-composed micro-XRF data sets obtained at HASYLAB, Beamline L were incorporated in the image: a micro-XRF 2D dynamic scan (height 175 × 20 μm, width: 122 × 20 μm) and a micro-XRF CT cross-section (width 165 × 20 μm) through the gill tissue, eggs, and gut. Zn density is the green channel, Ca density is the red channel, and Fe density is the blue channel. Reproduced, with permission, from [26] (A), [31] (Bi), [59] (Bii), [48] (C) and [55] (D).

3D-Raman Spectromicroscopy

Raman microscopy applications in biosciences have been recently reviewed [3] but without discussion of whether the technique is suitable for 3D histology. Thus, it is interesting to compare the IR and Raman techniques (Table 2). These techniques are usually considered as complementary in biosample analysis, although IR is more sensitive and Raman offers better lateral (i.e., along the z-axis) resolution (<1 μm) [13]. In principle, this property should give a significant advantage to Raman spectromicroscopy for resolving small tissue substructures [i.e., where the IR technique is already diffraction limited (<5–10 μm for the mid-IR range)]. However, this higher resolution is not easily exploitable. In fact, there are three major limits to Raman microscopy for the analysis of tissues: (i) the image data size becomes huge at high resolution (the data size for a 3D spectrum matrix should reach 11 TB for a 1-cm^3 tissue block at 10-μm resolution, and 1000× more at 1-μm resolution); (ii) the better the spatial resolution, the

Table 2. Major IR and Raman Band Assignments for Soft Tissues[a]

Vibrational mode (functional group)	IR frequency (cm^{-1})	Raman shift (cm^{-1})	Molecular information
Amide A, B	3300, 3100		Fermi resonance between N-H stretch and overtone of Amide II, sensitive to secondary structure
ν(-C=C-H) stretch	3010		Fatty acyl chains unsaturation
$\nu_{as}(-CH_3)$ stretch	2960	2960	Predominantly due to proteins
$\nu_{as}(-CH_3)$ stretch	2875	2932	Predominantly due to fatty acyl chains
$\nu_{as}(>CH_2)$ stretch	2924–2916	2880	Predominantly due to lipid, frequencies qualitatively
$\nu_{s}(-CH_3)$ stretch	2870		Predominantly due to lipid, frequencies qualitatively
$\nu_{s}(>CH_2)$ stretch	2855–2848	2850	Monitor acyl chain conformational order and packing
ν(>C=O)	1730–1760		Due to acid carbonyls
ν(>C=O)	1740–1720	1735	Due to ester carbonyl, sensitive to hydrogen bonding
Amide I	1685–1630	1670–1650	Predominantly due to C=O stretch, sensitive to secondary and tertiary structures
ν(>C=O)	1684, 1672, 1664, 1656, 1645, 1637, 1625, 1610		Proteins, β-turns, antiparallel β-sheets, parallel β-sheets, α-helix, unordered structure, α-like triple helix, antiparallel β-sheets, parallel β-sheets
ν(-C=C-)	Weak	1660–1600	Sensitive to conjugation
Amide II	1550–1530		Predominantly due to N-H in-plane bend and C-N stretch, sensitive to secondary structure
$\delta(>CH_2)$, $\delta(-CH_3)$	1475–1460	1452–1440	Methylene modes in IR sensitive to acyl chain packing
$\nu_{s}(>COO^{-})$	1450–1400	1420–1400	Due to NMF components and amino acid side chains
$\omega(>CH_2)$	1337		IR marker for Pro in collagen
$\tau(CH_2)$		1298	*Trans* acyl chain
Amide III	1275–1235	1270–1210	C-N stretch and N-H in-plane bend, sensitive to secondary structure
$\nu_{as}(P=O)$	1227		Phosphates
ν(C-C) skeletal		1130, 1060	*Trans* acyl chain
$\nu(PO_2^{-})$	1089	1090	DNA
ν(C-O-C)	1020–1040		Glucose (hemiacetal), glycogen α(1→4) glycosidic bonds
ν(C-C) aromatic ring		1003	Phenylalanine
ν(C-C)		940, 925, 880, 860	Collagen (Pro & HYP residues)
ν(C-C) pyrimidine ring		780	Cytosine
ν(C-C)		702, 605	Cholesterol

[a]Data from [6,12,26,29,31,32,38,40].

longer the acquisition duration, which can progressively lead to changes in ambient conditions between the moment of the background acquisition and the Raman spectra several hours later; and (iii) the better the spatial resolution, the smaller the organic material amount for each voxel and, thus, a lower S/N will be obtained. Therefore, analyzing tissue blocks at 1-μm resolution will alter the quantitative value of the chemical analysis performed. In addition, no study has yet provided an analytical demonstration of this approach. However, similarly to recent improvements in IR microscopy, an improvement in the sensitivity of detectors and/or the use of ultrafast lasers to speed up the acquisition of Raman spectra might re-equilibrate the analytical performances achieved by these two vibrational spectromicroscopy techniques for the analysis of large biosamples with 3D applications.

The main issue for the analysis of tissues is that modern Raman microscopes do not contain adapted optics that can analyze samples at 5–20-μm lateral resolutions. The optics currently used for Raman microscopy provide 200–500 nm resolution depending on lasers, further specializing this technology for use in nanophotonics. Thus, without the development of optics to adapt existing Raman microscopes for image acquisitions several microns in resolution, the issues raised through sample heating by lasers, data file size management, and acquisition time will not be easily overcome. Nevertheless, Raman spectromicroscopy has already been used for the 3D analysis of small biospecimens, mostly cells [12,38], while, for histology, it has been often used for 2D analyses, resulting in several diagnostic methods that have successfully detected tumors and metastases [39]. Thus, it is likely that Raman spectromicroscopy will have a role in the clinic in the future [40]. Another advantage of its high resolution is that it can be used to highlight subtle changes in small tissue substructures, such as endothelial dysfunctions induced by metastases [12], the abnormal inclusion of lipid droplets in cells [38], and so on.

On Raman spectra, the number of chemical parameters that can be extracted is smaller than that with IR spectra (Figure 1). The most-advanced studies for the analysis of tissues show that Raman spectra could provide up to 30–40 bands if an appropriate curve-fitting method is used [41]. Raw Raman spectra exhibit approximately 20 peaks, which is comparable to IR spectra. However, curve-fitting methods are rapidly limited by the noise level in the spectra, thus altering the resolution of many different bands from raw spectra. Although smoothing procedures may reject high-spatial frequency noise without introducing detectable nonlinearities [41], they also reduce the number of resolved bands. Therefore, both the limited laser power for nondestructive data acquisitions and the requirement for the fast analysis of large planar areas result in noisy Raman spectra, and only a few bands can be extracted for quantitative analyses based on a linear signal [42]. This observation reinforces the need to improve the technology so that Raman spectromicroscopy might become more routinely applicable to tissue block analysis.

3D-Mass Spectrometry Imaging

MSI techniques have two possible applications: the analysis of either inorganic or organic content through mass fractions [43]. In principle, MSI provides chemical data without labels and can perform 3D imaging with 1-μm lateral resolution or better, and with depth resolution down to a few nanometers. In general, MSI techniques include a spatially resolved ionization method to collect mass spectra from an array of positions across a sample [44,45]. Basically, two major types of MSI technique are used for tissue analysis: laser ablation inductively coupled plasma MS (LA-ICP-MS) imaging and ToF-SIMS imaging [46]. LA-ICP-MS imaging is best suited for analyzing inorganic content, while ToF-SIMS imaging is best for organic content. LA-ICP-MS offers the lowest limits of detection in the $mg.g^{-1}$ range [47], which is required for tissue content analyses. In practice, ToF-SIMS and LA-ICP-MS are well-established techniques that are used for molecular imaging under vacuum, which limits the development of the technique due to complicated and delicate sample preparations. However, ambient ionization methods, such as desorption electrospray ionization (DESI), have recently been introduced [48]. DESI-MSI has the advantages of not only ambient analyses, but also easier sample preparation and simplified analysis. In an effort to reconstruct a whole-mouse brain volume by DESI-MSI (Figure 2), the most abundant lipids of the organ could be detected in the negative-ion mode and reconstructed as a 3D image.

A compromise is sought between resolution, time of acquisition, and quality of spectral data for the 3D reconstruction of chemical parameters, with the result that, for 200 sections (out of 560 for the whole brain), only 36 20-μm-thick representative sections could be analyzed for 200-μm lateral resolution data acquisition. Mass scans lasted 1.16 s per pixel (67 min per section) for a total 40 h acquisition time to obtain a 3D model. From this 3D spectrum matrix of approximately 125 000 mass spectra, the most abundant ions in the mass spectra, m/z

834.4 and m/z 888.8, could be identified as the phosphatidylserines 18:0/22:6 (green in Figure 2) and the sulfatide 24:1 (red in Figure 2), respectively. The spectra extracted from a 2D section showed the two major peaks formed by these molecules and a series of small other peaks (approximately 18 identified, combining white and gray matter spectra for the 100–1100 m/z range).

The current state of the art is far from the submicron resolution potential of the technique, with large m/z data sets to exploit from the obtained 3D spectrum matrix. In fact, such a 3D imaging achievement, among other examples [49], shows the difficulties encountered by 3D-MSI for the analysis of large tissue blocks. The current limits of 3D-MSI for tissue analyses are as follows: (i) on a large tissue block, 3D-MSI produces only a few reliable peaks for quantitative molecular analyses; (ii) MSI does not analyze the complete tissue volume (ablation is a surface extraction procedure that does not include all the tissue material but just a fraction of it), thus restricting quantitative analyses in 3D; (iii) as for any other spectromicroscopy technique, the ability to extract given molecular parameters depends on the relative abundance of these chemical species 'as read in the spectra'; and (iv) MSI must *a priori* choose the m/z range to analyze, thus defining which molecular parameters are of interest for a tissue.

These factors limit the application of **nonsupervised analyses** to MSI. In fact, the more the sample is chemically complex and the larger the m/z range scanned, the more the mass spectrum becomes unreadable with a multitude of data, and there is little immediate correlation between these data to identify molecular entities [50]. Finally, with a softer fragmentation method, or by focusing on tissues that exhibit lower chemical complexity, reducing the number of peaks in mass spectra enables the reconstruction of some, but not many, molecular entities [51].

MSI is also able to quantitatively analyze metal ions in biological samples [52], which is a major analytical challenge considering the relatively weak concentrations of these chemical species. Metals are found in every cell, are present in more than 30% of proteins, and are essential for the function of most enzymes, yet their concentration remains low (Table 3). LA-ICP-MS imaging has no rival in metal analyses because it offers the highest sensitivity and, thus, allows quantitative rendering in 3D after image reconstruction from seriated tissue sections. The most problematic issue for metal imaging is the frequent contamination of tissues by exogenous metals in sampling steps, such as cryosectioning, deposition on substrates, and so on. Another concern for validating quantitative studies is that a destructive technique, such as LA-ICP-MS, does not allow any further measurement of the sample. However, this is true for all techniques currently available for analyzing metals in tissues [53].

Table 3. Concentration of Main Organic and Inorganic Contents in Several Mouse Organs[a]

Tissue	Fe (μg.g)	Cu (μg.g)	Zn (μg.g)	Water (%)	Lipids (%)	Proteins (%)	Polysaccharides (%)
Brain	15–30	1.1–2.1	6–15	68.5–82.6	5.3–18.1	10–11.5	0.2–0.4
Adipose	9–17	0.1–0.3	5–12	11.4–30.5	61.4–87.3	7–8.1	–
Muscle	160–190	0.3–1.7	28–45	70–78.6	1.6–6.8	17.9–21.3	0.2–0.6
Liver	220–280	1.6–5.0	30–44	72.8–75.8	1.5–7.8	16.1–19.6	0.4–0.6
Kidney	250–310	0.6–4.5	10–55	72.3–80. 5	2.8–6.9	15.8–19.9	0.1–0.2
Heart	280–380	5–13	20–33	71–80.9	2.4–10.1	15.9–18.2	0–0.1

[a]Data from [60,61].

3D X-Ray Fluorescence Microscopy

An alternative to MSI methods for analyzing trace elements and metal ions in biosamples is XRF imaging. A comprehensive review of metal ion imaging in biological samples was recently published [52], albeit without tackling the 3D application question. XRF imaging can detect trace elements in biological samples with submicron resolution. XRF spectra of a sample are obtained using electron beam, proton beam, or X-ray (photon) beam methods. Several biosamples could be scanned for 3D mapping, such as for a small part of the mouse brain [54], or smaller specimens (<1 mm^3), such as *Daphnia magna* [55] (Figure 2), *Caenorhabditis elegans* [56] or zebrafish embryos [57]. Compared with MSI, the development of nondestructive elemental imaging methods with XRF is feasible when an attenuated X-ray source is used to minimize the ionization on the sample. Recently, it was demonstrated that specimens of several mm^3 could be analyzed at resolutions down to 10–20 μm with a good sensitivity to reveal the distribution of several elements.

However, larger tissue blocks ($\sim$1 cm^3) have not yet been analyzed, due to the low sensitivity of the technique at histological resolutions. A 15-μm spatial resolution was achieved in the example shown in Figure 2, but this was for a biological specimen that presents a naturally high concentration contrast for Zn, Ca, and Fe ions, and several-folds higher than for soft tissues and organs found in vertebrates and mammals. Therefore, the applications of this technique for biosciences in general, or more specifically for biomedical and pharmaceutical research, are still limited. The development of more-sensitive detectors, rather than more-powerful sources (inducing harmful ionization in the sample), appears to be the way to enhance the 3D quantitative rendering of XRF spectromicroscopy for 3D histology.

The Technological Chain of 3D Chemical Imaging

With spectromicroscopy, the main issues for producing 3D chemical images are the sampling procedures, the management of S/N for obtaining reliable quantitative information throughout the 3D spectrum matrix, and the automation of most spectral data treatments for 3D image reconstruction. These issues will define the next generation of microscopes designed for developing 3D chemical imaging applications and the technical chain required for routine use by end-users who will not be spectroscopists, but rather physicians and biologists.

Here, the term ‘big data’ in 3D chemical imaging holds a double meaning, since a 3D spectrum matrix is at the same time massive and contains complex chemical information. The massive nature of the information is due to the huge number of spectra. However, the complex nature of this information stems from the fourth dimension of the voxels, the spectral data, which require advanced data treatments to extract the ‘embedded’ chemical information (e.g., individual absorption bands in IR and Raman spectra by curve-fitting methods). Furthermore, the analytic (i.e., the algorithms performing spectral data treatments to produce **biological metadata**) will require major computing resources, combining CPU means for high-performance calculation with GPU cards for both parallelized calculation on spectra and visualization of 3D reconstructed results.

Spectromics and Automation in 3D Chemical Imaging

Universal data treatment methods must be established for extracting chemical parameters provided by spectromicroscopies. This idea is paving the way to **spectromics**, the systematic and nonsupervised exploitation of all chemical data extracted from spectra, which was recently introduced for spectroscopies [26,58]. Spectral data treatments appear to be one of the most urgent issues to solve for developing any further 3D chemical imaging by spectromicroscopies. Expanding the concept of spectromics requires that chemical data derived from spectra (individual bands for IR and Raman, peaks for mass and XRF) can be used for the two different

analytical strategies: supervised analyses, where spectral data represent known chemical species or for reconstructing biological metadata of interest, and nonsupervised analyses, where spectral data are used for highlighting differences between samples or sample compartments (Figure 3).

As shown with IR spectro-microscopy and MSI, a supervised approach is required to reconstruct tissue substructures from its chemical contents. This requires cross-registration between the anatomical visualization of the sample and its chemical characterization by a spectromicroscopy method, thus combining histological (H&E, IHC, etc.) and chemical analyses. Briefly, the voxels corresponding to the substructure are selected and the chemical data are used to establish an exclusive chemical profile with all the other sample voxels. The nonsupervised approach exploits the whole set of chemical data extracted from spectra, without *a priori* knowledge. The two approaches are complementary by essence, but they must be used

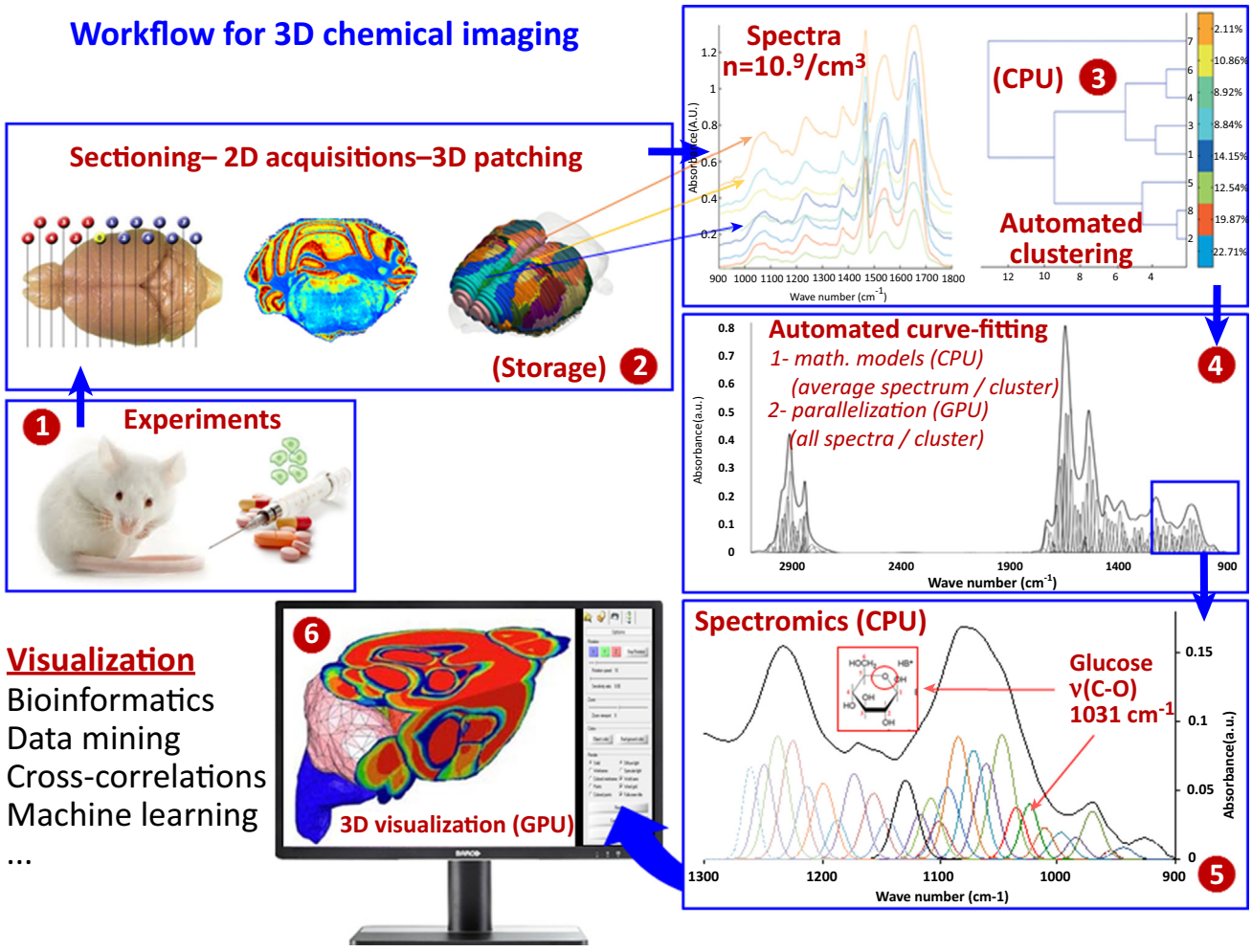

Figure 3. Workflow of High-Parallelization Process for High-Throughput (HT) Spectral Data Treatments on a Large 3D Spectrum Matrix. The 3D spectrum matrix can be split into homogeneous clusters of spectra presenting similar chemical profiles for HT parallelized calculation and extraction of chemical data. Robust mathematical models must be produced for minimizing the calculation workload in GPU-related parallelization steps. Steps are indicated by numbered red circles and referred in Box 2 and Figure360.
For a Figure360 author presentation of Figure 3, see the figure online at http://dx.doi.org/10.1016/j.tibtech.2017.08.002#mmc1

Box 2. Automating Spectra Curve-Fitting for 3D Chemical Imaging

Technologically, MSI and IR imaging appear close to reaching the expected analytical level for large-scale automated curve-fitting on 3D spectral images. With further technological improvements, highlighted below, Raman and XRF techniques are also likely reach the required analytical level: (i) A sensitivity (or S/N) level must be reached before curve-fitting methods can be developed for massive series of spectra. Curve-fitting must be performed on highly parallelized computing servers, which could prohibit any further quality checks of the results; (ii) The calculation workload on a large 3D spectrum matrix must be minimized. An organ usually comprises a few different substructures and cell phenotypes: thus, the clustering of spectra should provide a related number of clusters with relatively homogeneous chemical profiles (step 3 in Figure 3 in the main text); (iii) It is necessary to compare the raw spectra curve intensities (i.e., the intensity of absorptions for IR and Raman spectra, and the complete peak-picking intensities in mass and XRF spectra), which must be extracted automatically; (iv) The clustering of the whole set of spectra into highly homogeneous spectra families enables one to define a mathematical model per cluster (step 4 in Figure 3), although this results in a high CPU workload; and (v) The mathematical model obtained needs to be applied to all other spectra of its cluster to adjust the intensity, position, and shape parameters of all absorption bands. This process is highly parallelized on GPU calculation cards.

The production of 'biological metadata' from spectral data extracted as discussed above has been demonstrated for different tissue substructures. For example, such data are required to both identify the chemical profile to highlight the blood vessels compared with all other tissue content and to trace the contiguity of this chemical profile to reconstruct the solid object formed by the blood vessels in a 3D spectrum matrix. This introduces another degree of complexity in the analytical strategy (i.e., tracing the skeleton and volume of blood vessels, from thin capillaries to large arteries and veins). It also offers another opportunity to analyze more deeply the 3D features of the tissue block, thus generating 'secondary metadata'. The reconstruction of vessels as 3D solid objects will enable their geometrical parameters to be determined, such as their diameter, curvature, branching angles, and all other associated dimensions: also 'secondary metadata'.

according to an analytical strategy defined *ab initio*. In fact, the huge amount of data extracted from individual spectra and the heavy computing workload induced by their treatment in a large 3D spectrum matrix to reconstruct and visualize a result in 3D requires first defining the relevance of this analytical strategy.

In any case, spectromics requires extensive automation of data treatment steps. This is due to both the huge number of spectra that a 3D spectrum matrix may contain (millions to billions) and the lack of readability that a 3D spectrum matrix imposes, with voxels (thus spectra) representing chemical information that cannot be analyzed separately from adjacent voxels for reconstructing a substructure in 3D (Box 2).

This second generation of metadata derived from a 3D spectrum matrix is comparable to 3D histological analyses. As soon as the analytical technique provides a quantitative chemical analysis of tissue contents, the first and second generations of biological metadata can be subjected to cross-correlations; for example, in cancer research, the density of blood vessels can be analyzed with respect to the local concentration of metabolic parameters where tumor cells have been identified by their chemical profile [6]. This combination of chemical, anatomical, and substructure parameters from the same 3D chemical image of a sample is another unique analytical feature of spectromicroscopies.

Concluding Remarks

3D chemical imaging by spectromicroscopy could significantly expand our ability to perform analyses at the submicroscopic level if issues associated with the standardization of data acquisitions and treatment methods can be addressed (see Outstanding Questions). Several key features might be also generalized to all spectroscopies, such as the management of massive data from a high-resolution 3D spectrum matrix, which would require computing approaches that could be shared between techniques. Therefore, the future of these techniques for 3D histology will result from large networks of scientists working together to create the required technological chain of 3D chemical imaging. The use of such techniques in the biomedical and pharmaceutical fields might result from these new developments.

Outstanding Questions

Which spectroscopy techniques should be used for 3D chemical imaging?

What is the nature of expected chemical data that aids the 3D analysis of a tissue block? For elemental imaging, MSI and XRF imaging must be considered. For organic contents, MSI, Raman, and IR imaging will provide different chemical data.

What is the limit of tissue sectioning for 3D chemical imaging? To reconstruct small-tissue substructures in 3D, a tissue thickness of 3–5 μm is required. The issue then is to perform continuous sectioning of the tissue block without losing too many sections, which would affect the 3D reconstruction. In practice, this includes a large percentage of sections being lost. Thus, a 10-μm thickness is preferred.

What is the digital size of a 3D chemical image? A 3D spectral image has four dimensions: x, y, and z for the position of each voxel, and z' for the spectral data (with x' for wavenumber or m/z or keV values; y' for intensity). With several KBs per spectrum, a raw 3D spectrum matrix from a 1-cm^3 tissue block reaches approximately 10 TBs at a 5-μm resolution. This is a big-data issue that high-performance data analytics (HDPA) servers must solve.

What are the remaining issues for rendering 3D chemical imaging methods routine in the clinic?

What is a sufficiently high-throughput microscope? To achieve high reliability for 3D imaging, the microscopes producing spectral images must be able to not only threshold the S/N as a quality control tool, but also automate all acquisition and post-processing procedures.

What is the main way to make 3D chemical imaging reliable? To define the applicability of an analytical method for 3D chemical imaging, a compromise must be sought between an appropriate S/N and the resolution.

What is required of HPDA servers? The combination of storage and/or retrieval procedures and HPC with high parallelization on GPU cards is current hardware required for HPDA. This is critical for developing spectromics in 3D chemical imaging.

Acknowledgments

This study was supported by the French 'Agence Nationale de la Recherche' and the Taiwanese 'Ministry of Sciences and Techniques' (ANR and MOST – contract 'Tecsan n°2013-001-3DXIR-Pathology'), and the Banque Publique d'Investissement (BPI – PIACISN2-GDN2015 – ImpactTumors).

References

1. Hjornevik, T. *et al.* (2007) Three-dimensional atlas system for mouse and rat brain imaging data. *Front. Neuroinform.* 1, 4
2. Liu, Y.C. and Chiang, A.S. (2003) High-resolution confocal imaging and three-dimensional rendering. *Methods* 30, 86–93
3. Matousek, P. and Stone, N. (2016) Development of deep subsurface Raman spectroscopy for medical diagnosis and disease monitoring. *Chem. Soc. Rev.* 45, 1794–1802
4. Mounicou, S. *et al.* (2009) Metallomics: the concept and methodology. *Chem. Soc. Rev.* 38, 1119–1138
5. Aichler, M. and Walch, A. (2015) MALDI Imaging mass spectrometry: current frontiers and perspectives in pathology research and practice. *Lab. Invest.* 95, 422–431
6. Petibois, C. and Desbat, B. (2010) Clinical application of FTIR imaging: new reasons for hope. *Trends Biotechnol.* 28, 495–500
7. Chen, H.H. *et al.* (2016) The future of infrared spectroscopy in biosciences: *in vitro*, time-resolved, and 3D. *Acta Phys. Pol. A* 129, 255–259
8. Martin, M.C. *et al.* (2013) 3D spectral imaging with synchrotron Fourier transform infrared spectro-microtomography. *Nat. Methods* 10, 861–864
9. Kubota, H. *et al.* (2003) Development of a micro-FT-IR system for three-dimensional structural studies. *Vib. Spectrosc.* 31, 11–17
10. Wood, B.R. *et al.* (2006) A three-dimensional multivariate image processing technique for the analysis of FTIR spectroscopic images of multiple tissue sections. *BMC Med. Imaging* 6, 1–9
11. Chen, X. *et al.* (2015) Quantitative 3D molecular cutaneous absorption in human skin using label free nonlinear microscopy. *J. Control. Release* 200, 78–86
12. Pacia, M.Z. *et al.* (2016) 3D Raman imaging of systemic endothelial dysfunction in the murine model of metastatic breast cancer. *Anal. Bioanal. Chem.* 408, 3381–3387
13. Yao, S. *et al.* (2013) The role of asbestos morphology on their cellular toxicity: an *in vitro* 3D Raman/Rayleigh imaging study. *Anal. Bioanal. Chem.* 27, 8701–8707
14. Clarke, G.M. *et al.* (2012) 3D pathology volumetric technique: a method for calculating breast tumour volume from whole-mount serial section images. *Int. J. Breast Cancer* 2012, 691205
15. Giordano, S. *et al.* (2016) 3D mass spectrometry imaging reveals a very heterogeneous drug distribution in tumors. *Sci. Rep.* 6, 37027
16. Stille, M. *et al.* (2013) 3D reconstruction of 2D fluorescence histology images and registration with *in vivo* MR images: application in a rodent stroke model. *J. Neurosci. Methods* 219, 27–40
17. Bourassa, D. *et al.* (2014) 3D imaging of transition metals in the zebrafish embryo by X-ray fluorescence microtomography. *Metallomics* 6, 1648–1655
18. Garrevoet, J. *et al.* (2014) Methodology toward 3D micro X-ray fluorescence imaging using an energy dispersive charge-coupled device detector. *Anal. Chem.* 86, 11826–11832
19. Nakano, K. and Tsuji, K. (2010) Development of laboratory confocal 3D-XRF spectrometer and nondestructive depth profiling. *J. Anal. At. Spectrom.* 25, 562–569
20. Petibois, C. (2010) Imaging methods for elemental, chemical, molecular, and morphological analyses of single cells. *Anal. Bioanal. Chem.* 397, 2051–2065
21. Rogalski, A. (2012) Progress in focal plane array technologies. *Prog. Quantum Technol.* 36, 342–473
22. Wang, Y. *et al.* (2015) Three-dimensional reconstruction of light microscopy image sections: present and future. *Front. Med.* 9, 30–45
23. Petibois, C. and Déléris, G. (2006) Chemical mapping of tumor progression by FT-IR imaging: towards molecular histopathology. *Trends Biotechnol.* 24, 455–462
24. Tiwari, S. *et al.* (2016) Towards translation of discrete frequency infrared spectroscopic imaging for digital histopathology of clinical biopsy samples. *Anal. Chem.* 88, 10183–10190
25. Ogunleke, A. *et al.* (2017) Fourier-transform vs. quantum-cascade-laser infrared microscopes for histo-pathology: from lab to hospital? *Trends Anal. Chem.* 89, 190–196
26. Bobroff, V. *et al.* (2017) 3D digital histology by quantitative IR microscopy and spectromics. *J. Biophotonics* 10, 598–606
27. Petibois, C. *et al.* (2014) *Method for determining absorption band in spectrum for three-dimensional imaging of e.g., cell for microscopic examination of tissue, involves using residual spectrum as calculation spectrum, and outputting extracted absorption band,* Inserm, ed)
28. Petibois, C. *et al.* (2014) *Method for correcting infrared (IR) absorption spectrum, involves correcting first baseline correction curve in accordance with results of comparing step and subtracting corrected baseline correction curve from measured spectrum,* Inserm, ed)
29. Goormaghtigh, E. *et al.* (2009) Protein secondary structure content in solution, films and tissues: redundancy and complementarity of the information content in circular dichroism, transmission and ATR FTIR spectra. *Biochim. Biophys. Acta* 1794, 1332–1343
30. Hu, Y. *et al.* (2005) Resolving overlapped spectra with curve fitting. *Spectrochim. Acta A Mol. Biomol. Spectrosc.* 62, 16–21
31. Bobroff, V. *et al.* (2016) FTIR spectroscopy characterization of fatty-acyl-chain conjugates. *Anal. Bioanal. Chem.* 407, 1–6
32. Derenne, A. *et al.* (2014) Lipid quantification method using FTIR spectroscopy applied on cancer cell extracts. *Biochim. Biophys. Acta* 1841, 1200–1209
33. Hsu, H.S. *et al.* (2002) Ultrastructural and biophysical studies on protein conformations of epithelium and stroma in benign prostatic hyperplasia before and after transurethral resection of the prostate. *Ultrastruct. Pathol.* 26, 137–141
34. Troullier, A. *et al.* (2000) Transient non-native secondary structures during the refolding of alpha-lactalbumin detected by infrared spectroscopy. *Nat. Struct. Biol.* 7, 78–86
35. Belbachir, K. *et al.* (2011) Orientation of molecular groups of fibers in nonoriented samples determined by polarized ATR-FTIR spectroscopy. *Anal. Bioanal. Chem.* 401, 3263–3268
36. Benard, A. *et al.* (2014) Infrared imaging in breast cancer: automated tissue component recognition and spectral characterization of breast cancer cells as well as the tumor microenvironment. *Analyst* 139, 1044–1056
37. Smolina, M. and Goormaghtigh, E. (2016) FTIR imaging of the 3D extracellular matrix used to grow colonies of breast cancer cell lines. *Analyst* 141, 620–629
38. Majzner, K. *et al.* (2014) Raman imaging providing insights into chemical composition of lipid droplets of different size and origin: in hepatocytes and endothelium. *Anal. Chem.* 86, 6666–6674
39. Stone, N. and Matousek, P. (2008) Advanced transmission Raman spectroscopy: a promising tool for breast disease diagnosis. *Cancer Res.* 68, 4424–4430
40. Freudiger, C.W. *et al.* (2012) Multicolored stain-free histopathology with coherent Raman imaging. *Lab. Invest.* 92, 1492–1502
41. Vickers, T.J. *et al.* (2001) Curve fitting and linearity: data processing in raman spectroscopy. *Appl. Spectrosc.* 55, 389–393
42. Brauns, E.B. and Meier, R.J. (2009) Issues in curve fitting vibrational spectra: bandshape justification and the influence of background correction. *Vib. Spectrosc.* 49, 303–304
43. Becker, J.S. and Jakubowski, N. (2009) The synergy of elemental and biomolecular mass spectrometry: new analytical strategies in life sciences. *Chem. Soc. Rev.* 38, 1969–1983

44. Zimmerman, T.A. *et al.* (2008) Imaging of cells and tissues with mass spectrometry: adding chemical information to imaging. *Methods Cell Biol.* 89, 361–390
45. Fornai, L. *et al.* (2012) Three-dimensional molecular reconstruction of rat heart with mass spectrometry imaging. *Anal. Bioanal. Chem.* 404, 2927–2938
46. Fletcher, J.S. (2015) Latest applications of 3D ToF-SIMS bioimaging. *Biointerphases* 10, 018902
47. Becker, J.S. *et al.* (2014) Bioimaging mass spectrometry of trace elements – recent advance and applications of LA-ICP-MS: a review. *Anal. Chim. Acta* 835, 1–18
48. Eberlin, L.S. *et al.* (2010) Three-dimensional vizualization of mouse brain by lipid analysis using ambient ionization mass spectrometry. *Angew. Chem. Int. Ed. Engl.* 49, 873–876
49. Hare, D.J. *et al.* (2012) Three-dimensional atlas of iron, copper, and zinc in the mouse cerebrum and brainstem. *Anal. Chem.* 84, 3990–3997
50. Norris, J.L. *et al.* (2016) Pathology interface for the molecular analysis of tissue by mass spectrometry. *J. Pathol. Inform.* 7, 13
51. Becker, J.S. *et al.* (2011) Mass spectrometric imaging (MSI) of metals using advanced BrainMet techniques for biomedical research. *Int. J. Mass Spectrom.* 307, 3–15
52. Hare, D.J. *et al.* (2015) Imaging metals in biology: balancing sensitivity, selectivity and spatial resolution. *Chem. Soc. Rev.* 44, 5941–5958
53. Hare, D.J. *et al.* (2010) Three-dimensional elemental bio-imaging of Fe, Zn, Cu, Mn and P in a 6-hydroxydopamine lesioned mouse brain. *Metallomics* 2, 745–753
54. Ciccotosto, G.D. *et al.* (2014) Quantitation and localization of intracellular redox active metals by X-ray fluorescence microscopy in cortical neurons derived from APP and APLP2 knockout tissue. *Metallomics* 6, 1894–1904
55. De Samber, B. *et al.* (2008) Three-dimensional elemental imaging by means of synchrotron radiation micro-XRF: developments and applications in environmental chemistry. *Anal. Bioanal. Chem.* 390, 267–271
56. McColl, G. *et al.* (2012) *Caenorhabditis elegans* maintains highly compartmentalized cellular distribution of metals and steep concentration gradients of manganese. *PLoS One* 7, e32685
57. Fahrni, C.J. (2007) Biological applications of X-ray fluorescence microscopy: exploring the subcellular topography and speciation of transition metals. *Curr. Opin. Chem. Biol.* 11, 121–127
58. Arlinghaus, H.F. *et al.* (2006) Mass spectrometric characterization of elements and molecules in cell cultures and tissues. *Appl. Surf. Sci.* 252, 6941–6948
59. Rani, A. *et al.* (2016) Trimethylamine-N-oxide switches from stabilizing nature: a mechanistic outlook through experimental techniques and molecular dynamics simulation. *Sci. Rep.* 6, 23656
60. Forbes, R.M. *et al.* (1953) The composition of the adult human body as determined by chemical analysis. *J. Biol. Chem.* 203, 359–366
61. Mitchell, H.H. *et al.* (1945) The chemical composition of the adult human body and its bearing on the biochemistry of growth. *J. Biol. Chem.* 158, 625–637